Boundary homogenization for trapping patchy particles

Sean D. Lawley [*]

Department of Mathematics, University of Utah, Salt Lake City, Utah 84112, USA

Many systems in chemical and biological physics involve diffusing particles being trapped by absorbing patches on otherwise reflecting surfaces. Such systems are commonly studied by boundary homogenization, in which the heterogenous boundary condition on the patchy surface is replaced by a uniform boundary condition involving a single parameter which encapsulates the effective trapping properties of the surface. In prior works on boundary homogenization, the surface is patchy and the diffusing particles are homogeneous. In this paper, we consider the opposite scenario in which a homogenous surface traps patchy particles, which could model proteins with localized binding sites, cells with membrane receptors, or patchy colloids or nanoparticles. We derive an explicit formula for the effective trapping rate which reveals a fundamental interplay between the translational and rotational diffusivities of the patchy particle, a phenomenon not typically seen in boundary homogenization. Motivated by receptors on the cell membrane, our analysis also allows for the possibility that the patches diffuse on the surface of the particle. We formulate the system in terms of a high-dimensional, time-dependent, anisotropic diffusion equation and employ matched asymptotic analysis to derive the effective trapping rate. We confirm our results by detailed numerical simulations.

I. INTRODUCTION

Many systems in chemical and biological physics involve diffusing particles binding to heterogeneous or "patchy" surfaces. Examples include chemicals binding to receptors on a cell membrane [1], reactions on porous catalyst support structures [2], diffusion current to collections of microelectrodes [3], and water transpiration through plant stomata [4,5]. Such patchy surfaces are often modeled as reflecting surfaces covered by absorbing patches or traps, see Fig. 1(a).

In such a model, it is common to replace the heterogeneous surface by a homogenized surface involving a single "trapping rate" $\kappa > 0$ which encapsulates the effective reactivity or permeability of the original heterogeneous surface. Indeed, many works have derived formulas for such trapping rates which depend on various characteristics of the patchy surface, such as the fraction of the surface covered in traps, the sizes and shapes of traps, the arrangement of traps, etc. [6–14].

The idea behind homogenizing patchy surfaces is that, due to particle diffusion in the directions parallel to the surface, the surface heterogeneity only affects the diffusing particle concentration near the surface. In particular, the concentration is constant in directions parallel to the surface outside a boundary layer, where the width of this layer depends on the length scale of the surface heterogeneity.

Hence, if one is interested in the concentration outside this layer, then the particle concentration, $c(x, t)$, at time t depends only on the one-dimensional distance $x > 0$ from the surface. In this framework, the surface heterogeneity is approximated by an effective trapping rate $\kappa > 0$ used in a homogenized boundary condition at the surface,

$$D_{\text{tr}} \frac{\partial}{\partial x} c = \kappa c, \quad x = 0, \tag{1}$$

where D_{tr} is the translational diffusivity of the particles. Notice that small (large) values of κ correspond to a surface that is mostly reflecting (absorbing).

In prior works on boundary homogenization, the trapping surface is patchy and the diffusing particles are assumed to be homogeneous [6–14]. In this paper, we consider the opposite scenario in which patchy particles bind to a homogenous surface, see Fig. 1(b). In this case, the patchy particle could represent a protein [15], a patchy colloid or nanoparticle [16,17], or a cell [1]. Indeed, the ability of cells to bind to surfaces through adhesion molecules on their membranes is critical to many physiological processes and is also used in biotechnology [18].

In our model, a patchy particle binds to the surface when one of its patches makes contact with the surface; otherwise, the particle reflects from the surface. That is, binding requires a certain particle orientation on contact with the surface. For this model, we derive an explicit formula for the effective trapping rate κ.

To briefly summarize our results, consider a diffusing spherical particle (macromolecule) of radius R. Suppose the particle is covered by $N \geqslant 1$ locally circular patches of radius $a \ll R$ which are approximately evenly distributed. The particle's distance from the surface is governed by its translational diffusivity, D_{tr}, and its orientation is governed by its rotational diffusivity, D_{rot}. Motivated by receptors which diffuse on the cell membrane [18], we also allow for the possibility that the patches diffuse on the surface of the particle with diffusivity $D_{\text{pat}} \geqslant 0$ [see Fig. 1(b)]. We show that the particle binding (i.e., trapping) at the surface is well approximated by the
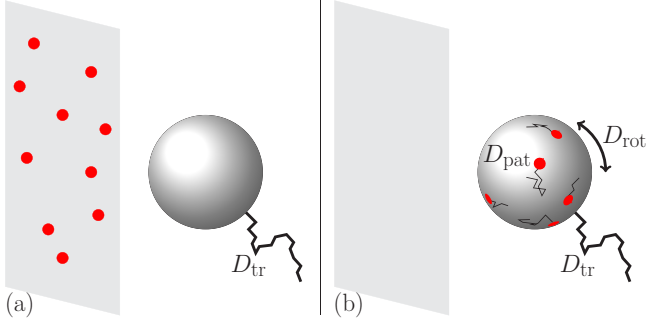
---

[*]lawley@math.utah.edu

FIG. 1. (a) A homogeneous particle and a patchy surface. The particle binds to the surface if it touches one of the red patches on the surface. (b) A patchy particle and a homogeneous surface. The particle binds to the surface if one of its patches touches the surface. In both (a) and (b), the particle has translational diffusivity D_{tr}. In (b), the particle's rotational diffusivity D_{rot} plays a crucial role in binding. Further, the patches in (b) diffuse on the surface of the particle with diffusivity D_{pat}.

boundary condition (1) with trapping rate

$$\kappa = \frac{Na}{\pi R^2}\sqrt{D_{tr}(R^2 D_{rot} + D_{pat})}. \qquad (2)$$

The rest of the paper is organized as follows. In Sec. II, we formulate our model and derive a high-dimensional, time-dependent, anisotropic diffusion equation describing the system. We then apply matched asymptotic analysis to this partial differential equation (PDE) in Sec. III to obtain the trapping rate in (2). In Sec. IV, we verify our results by numerical simulations. In Sec. V, we discuss the parameter regimes and geometries in which boundary homogenization with the trapping rate in (2) is valid. We conclude by discussing relations to prior work.

II. MODEL FORMULATION

Consider a spherical particle (macromolecule) with radius $R > 0$ in a one-dimensional slab of either finite or infinite width $L + 2R$, where $0 < L \leqslant \infty$. Suppose the particle diffuses with both translational diffusivity and rotational diffusivity, see Fig. 1(b). Suppose the particle reflects from the right wall of the slab (if $L < \infty$). Furthermore, suppose the particle either reflects or is absorbed at the left wall of the slab, depending on the orientation of the particle and its surface patches when it makes contact with the wall. In particular, the particle is absorbed when one of its patches touches the left wall.

To analyze this system, we center our reference frame on the particle and allow the reference frame to rotate with the particle's rotational diffusion, see Fig. 2. It follows that the point on the left wall that is closest to the particle diffuses in the annulus,

$$\{\mathbf{x} \in \mathbb{R}^3 : R \leqslant |\mathbf{x}| \leqslant L + R\}.$$

We denote the position of this point at time $t \geqslant 0$ in the spherical coordinates,

$$(X(t), \Theta_0(t), \Phi_0(t)) \in [R, L + R] \times [0, \pi) \times [0, 2\pi). \quad (3)$$

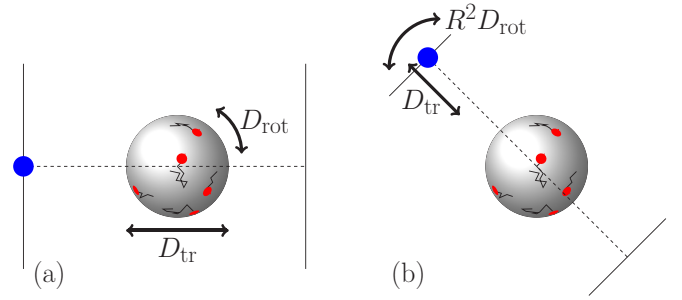

FIG. 2. (a) Particle diffusing in a one-dimensional slab. The particle orientation is governed by D_{rot} and its horizontal motion is governed by D_{tr} (motion in other directions is irrelevant). The blue ball depicts the closest point on the left wall of the slab. (b) Centering the reference frame on the particle and letting the reference frame rotate with the particle, it follows that the blue ball diffuses in an annulus about the particle. The angular diffusion of the blue ball is governed by D_{rot} and its distance from the particle is governed by D_{tr}. In both (a) and (b), the patches diffuse on the particle with diffusivity D_{pat}.

If we denote the translational and rotational diffusivities of the particle by $D_{tr} > 0$ and $D_{rot} \geqslant 0$, then it follows that the stochastic process in (3) satisfies the following stochastic differential equations (SDEs):

$$dX(t) = \sqrt{2D_{tr}}\, dW_X(t),$$

$$d\Theta_0(t) = \frac{D_{rot}}{\tan[\Theta_0(t)]}\, dt + \sqrt{2D_{rot}}\, dW_{\Theta_0}(t), \qquad (4)$$

$$d\Phi_0(t) = \frac{\sqrt{2D_{rot}}}{\sin[\Theta_0(t)]}\, dW_{\Phi_0}(t),$$

where W_X, W_{Θ_0}, and W_{Φ_0} are independent standard Brownian variables. Notice that the diffusion of $X(t)$ is governed by D_{tr}, while the diffusion of $(\Theta_0(t), \Phi_0(t))$ is governed by D_{rot} (see Fig. 2).

We suppose that the particle carries $N \geqslant 1$ patches on its surface, which diffuse independently on the surface with diffusivity $D_{pat} \geqslant 0$. We assume

$$R^2 D_{rot} + D_{pat} > 0.$$

(We discuss the trivial case $R^2 D_{rot} + D_{pat} = 0$ in Sec. V B.) To describe the patches, define the spherical cap

$$\Gamma(p, \varepsilon) := \{(R, \theta, \varphi) : (\theta - \theta_p)^2 + \sin^2(\theta_p)(\varphi - \varphi_p)^2 \leqslant \varepsilon^2\},$$

centered at a point p with spherical coordinates

$$p = (R, \theta_p, \varphi_p) \in \{R\} \times [0, \pi) \times [0, 2\pi).$$

Notice that $\varepsilon > 0$ is the angle between (a) the ray from the center of the particle to the apex of the cap and (b) the ray from the center of the particle to the edge of the base of the cap.

The N patches are then the spherical caps $\{\Gamma(P_n(t), \varepsilon b_n)\}_{n=1}^N$, where

$$P_n(t) = (R, \Theta_n(t), \Phi_n(t)), \quad n \in \{1, \dots, N\}, \qquad (5)$$

is the center of the nth patch at time $t \geqslant 0$. Here we have introduced the constants $\{b_n\}_{n=1}^N$ with $b_n = \mathcal{O}(1)$ to allow the

patches to have different sizes. Since the surface area of the nth patch is

$$\pi(\varepsilon b_n R)^2 + \mathcal{O}(\varepsilon^3) \quad \text{for } \varepsilon \ll 1,$$

we refer to $\varepsilon b_n R$ as the radius of the nth patch.

Since we allow the patches to diffuse independently on the surface of the particle, it follows that the spherical coordinates of the center of the nth patch in (5) follow the SDEs,

$$d\Theta_n(t) = \frac{D_{\text{pat}}}{R^2 \tan[\Theta_n(t)]} \, dt + \frac{\sqrt{2D_{\text{pat}}}}{R} \, dW_{\Theta_n}(t),$$

$$d\Phi_n(t) = \frac{\sqrt{2D_{\text{pat}}}}{R \sin[\Theta_n(t)]} \, dW_{\Phi_n}(t), \quad n \in \{1, \dots, N\},$$

(6)

where $\{W_{\Theta_n}\}_{n=1}^N$ and $\{W_{\Phi_n}\}_{n=1}^N$ are independent standard Brownian variables. Note that we have assumed in (6) that the patches are noninteracting, and thus they could overlap and diffuse through each other. Note also that patch diffusion ($D_{\text{pat}} > 0$) ensures that the patches become uniformly distributed as time increases, regardless of their initial arrangement. If $D_{\text{pat}} = 0$, then we assume that the patches are approximately evenly distributed.

To summarize, if we define the sets

$$\Omega := (R, L + R) \times \Omega_0^{N+1}, \quad \Omega_0 := [0, \pi) \times [0, 2\pi),$$

then the state of the entire system at time $t \geqslant 0$ lies in the closure of Ω,

$$(X(t), \Theta(t), \Phi(t)) \in \overline{\Omega}, \quad (7)$$

where $\Theta(t)$ and $\Phi(t)$ denote the vectors,

$$\Theta(t) = (\Theta_0(t), \Theta_1(t), \dots, \Theta_N(t)) \in [0, \pi)^{N+1},$$

$$\Phi(t) = (\Phi_0(t), \Phi_1(t), \dots, \Phi_N(t)) \in [0, 2\pi)^{N+1}.$$

We analyze the so-called survival probability of this system, which is the probability that the particle has not become bound by time $t \geqslant 0$.

To describe the survival probability, let $\tau \geqslant 0$ be the first time that the particle binds to the left wall,

$$\tau := \inf\left\{ t \geqslant 0 : (X(t), \Theta_0(t), \Phi_0(t)) \in \bigcup_{n=1}^N \Gamma(P_n(t), \varepsilon b_n) \right\}.$$

(8)

The survival probability is then the probability that the particle has not become bound before time $t \geqslant 0$,

$$S(x, \theta, \varphi, t) := \mathbb{P}(\tau > t \mid X(0) = x, \Theta(0) = \theta, \Phi(0) = \varphi),$$

(9)

where θ and φ denote the vectors

$$\theta = (\theta_0, \theta_1, \dots, \theta_N) \in [0, \pi)^{N+1},$$

$$\varphi = (\varphi_0, \varphi_1, \dots, \varphi_N) \in [0, 2\pi)^{N+1}.$$

(10)

We emphasize that the survival probability (9) is conditioned on the initial state $X(0) = x$, $\Theta(0) = \theta$, $\Phi(0) = \varphi$. Throughout the paper, we use the capital letters (X, Θ, Φ) to denote the time-dependent values of the stochastic process in (7), and we use the lowercase letters (x, θ, φ) to denote the arguments of the survival probability $S(x, \theta, \varphi, t)$ [which are initial conditions of the stochastic process in (7)].

The survival probability satisfies the backward Kolmogorov equation [19] (or backward Fokker-Planck equation [20]), which in this case is

$$\partial_t S = \mathbb{L}S, \quad (x, \theta, \varphi) \in \Omega, \, t > 0, \quad (11)$$

where

$$\mathbb{L} := D_{\text{tr}} \partial_{xx} + D_{\text{rot}} \mathcal{L}_0 + R^{-2} D_{\text{pat}} \sum_{n=1}^N \mathcal{L}_n,$$

and $\mathcal{L}_n$ is the Laplace-Beltrami operator acting on the nth angular coordinates (θ_n, φ_n) for $n \in \{0, 1, \dots, N\}$,

$$\mathcal{L}_n := [\sin(\theta_n)]^{-2} \partial_{\varphi_n \varphi_n} + \cot(\theta_n) \partial_{\theta_n} + \partial_{\theta_n \theta_n}.$$

We emphasize that the diffusion operators in (11) act anisotropically. In particular, the operator $\partial_{xx} + \mathcal{L}_0$ is not the Laplacian in spherical coordinates (x, θ_0, φ_0) (see Fig. 2).

To complete the boundary value problem satisfied by S, first note that S satisfies the following initial condition by definition:

$$S = 1, \quad (x, \theta, \varphi) \in \Omega, \, t = 0. \quad (12)$$

Next, since the particle reflects from the right wall of the slab in the case $L < \infty$, we obtain a no-flux boundary condition at $x = L + R$,

$$\partial_x S = 0, \quad x = L + R, \, (\theta, \varphi) \in \Omega_0^{N+1}, \, t > 0. \quad (13)$$

That is, (13) holds when $x = L + R$, regardless of the value of the angles (θ, φ) in (10). In the case $L = \infty$, (13) is replaced by

$$\lim_{x \to \infty} S = 1, \quad (\theta, \varphi) \in \Omega_0^{N+1}, \, t > 0, \quad (14)$$

since the probability that the particle reaches the left wall in any fixed finite time $t > 0$ vanishes in the limit that the particle starts infinitely far from the left wall.

If one of the patches on the particle touches the left wall, then it is immediately absorbed. Otherwise, the particle reflects from the left wall. Hence, we obtain the mixed boundary conditions at $x = R$,

$$S = 0, \quad x = R, \, (\theta_0, \varphi_0) \in \cup_{n=1}^N \Gamma(p_n, \varepsilon b_n),$$

$$\partial_x S = 0, \quad x = R, \, (\theta_0, \varphi_0) \notin \cup_{n=1}^N \Gamma(p_n, \varepsilon b_n),$$

(15)

where p_n denotes the initial center of the nth patch,

$$p_n := (R, \theta_n, \varphi_n).$$

In words, the first boundary condition in (15) means that if the particle is initially placed at the left wall ($x = R$) and one of the patches is initially aligned so that it touches the wall $[(\theta_0, \varphi_0) \in \cup_{n=1}^N \Gamma(p_n, \varepsilon b_n)]$, then the particle immediately binds, and so $S = 0$.

In the limit that the patches are small ($\varepsilon \ll 1$), we show below that the solution $S(x, \theta, \varphi, t)$ to this $(2N + 3)$-dimensional problem is well approximated by the solution $\overline{S}(x, t)$ of the following one-dimensional problem,

$$\partial_t \overline{S} = D_{\text{tr}} \partial_{xx} \overline{S}, \quad x \in (R, L + R), \, t \geqslant 0, \quad (16)$$

with initial condition $\overline{S} = 1$ and boundary condition,

$$D_{\text{tr}} \partial_x \overline{S} = \kappa \overline{S}, \quad x = R, \quad (17)$$

where $\kappa > 0$ is the effective trapping rate we derive below. Naturally, $\overline{S}$ satisfies either (13) or (14), depending if $L < \infty$ or $L = \infty$.

III. MATHEMATICAL ANALYSIS

A. Matched asymptotic analysis

Since the particle becomes perfectly reflecting as $\varepsilon \to 0$, it is immediate that

$$\lim_{\varepsilon \to 0} S(x, \theta, \varphi, t) = 1, \qquad (18)$$

for each $(x, \theta, \varphi) \in \Omega$ and $t \geqslant 0$. To obtain more information about the behavior of S as $\varepsilon \to 0$, we employ matched asymptotic analysis, adapting the approach of Refs. [12,21] (see also Refs. [22–29]). In particular, we expect that S has a boundary layer in a neighborhood of each of the patches. Hence, we introduce the outer expansion which is valid away from the patches,

$$S \sim 1 + \varepsilon S_1 + \cdots, \qquad (19)$$

for some function $S_1(x, \theta, \varphi, t)$.

Plugging the outer expansion (19) into (11)–(15) implies that S_1 satisfies

$$\partial_t S_1 = \mathbb{L} S_1, \quad (x, \theta, \varphi) \in \Omega, \quad t > 0,$$
$$\partial_x S_1 = 0, \quad x = R, \quad (\theta_0, \varphi_0) \notin \cup_{n=1}^N \{(\theta_n, \varphi_n)\}. \quad (20)$$

Notice that from the perspective of the outer solution, the patches have become points. The analysis below yields the singular behavior of S_1 as $(x, \theta_0, \varphi_0) \to (R, \theta_n, \varphi_n)$.

In the inner region near the nth patch, we introduce the local coordinates (η, s_1, s_2) defined by

$$\eta = \varepsilon^{-1}(x/R - 1),$$
$$s_1 = \varepsilon^{-1} \beta^{-1} \sin(\theta_n)(\varphi_0 - \varphi_n),$$
$$s_2 = \varepsilon^{-1} \beta^{-1}(\theta_0 - \theta_n),$$

where β is the dimensionless constant,

$$\beta := \sqrt{\frac{R^2 D_{\text{rot}} + D_{\text{pat}}}{D_{\text{tr}}}} > 0. \qquad (21)$$

We then define the inner solution w as a function of local coordinates,

$w(\eta, s_1, s_2, \theta', \varphi', t)$

$\quad := S_1(R + \varepsilon R \eta, \varphi_n + \varepsilon \beta(\sin \theta_n)^{-1} s_1, \theta_n + \varepsilon \beta s_2, \theta', \varphi', t),$

where $(\theta', \varphi') = (\theta_1, \varphi_1, \dots, \theta_N, \varphi_N)$.

By our choice of β in (21), a quick calculation shows that the differential operator $\mathbb{L}$ in (11) expressed in local coordinates is

$$\mathbb{L} = \varepsilon^{-2} R^{-2} D_{\text{tr}} \left(\partial_{\eta\eta} + \partial_{s_1 s_1} + \partial_{s_2 s_2} \right) + \mathcal{O}(\varepsilon^{-1}).$$

Therefore, plugging the inner expansion

$$w = w_0 + \varepsilon w_1 + \cdots$$

into (11) implies that w_0 is constant in time and harmonic in upper half-space,

$$\left(\partial_{\eta\eta} + \partial_{s_1 s_1} + \partial_{s_2 s_2} \right) w_0 = 0, \quad \eta > 0, \; s_1 \in \mathbb{R}, \; s_2 \in \mathbb{R}.$$

Furthermore, (15) implies that w_0 satisfies the following boundary conditions on the $\eta = 0$ plane:

$$\partial_\eta w_0 = 0, \quad \text{on } \eta = 0, \quad s_1^2 + s_2^2 \geqslant (b_n/\beta)^2,$$
$$w_0 = 0, \quad \text{on } \eta = 0, \quad s_1^2 + s_2^2 \leqslant (b_n/\beta)^2.$$

This problem for w_0 can be solved explicitly using the solution to the so-called electrified disk problem from electrostatics [30], derived by Weber [31] in 1873. From this explicit solution, it follows that w_0 has the far-field behavior,

$$w_0 \sim A \left(1 - \frac{2b_n}{\pi \beta \rho} \right), \quad \text{as } \rho := \sqrt{\eta^2 + s_1^2 + s_2^2} \to \infty, \qquad (22)$$

where A is a constant to be determined by matching to the outer solution.

The matching condition is that the near-field behavior of the outer expansion as $(x, \theta_0, \varphi_0) \to (R, \theta_n, \varphi_n)$ must agree with the far-field behavior of the inner expansion as $\rho \to \infty$. That is,

$$1 + \varepsilon S_1 + \cdots \sim w_0 + \varepsilon w_1 + \cdots,$$
$$\text{as } (x, \theta_0, \varphi_0) \to (R, \theta_n, \varphi_n), \; \rho \to \infty. \qquad (23)$$

Plugging (22) into (23) implies that $A = 1$ and that S_1 has the following singular behavior as $(x, \theta_0, \varphi_0) \to (R, \theta_n, \varphi_n)$:

$$S_1 \sim \frac{-2b_n/\pi}{\sqrt{\beta^2 \left(\frac{x}{R} - 1 \right)^2 + \sin^2(\theta_n)(\varphi_0 - \varphi_n)^2 + (\theta_0 - \theta_n)^2}}.$$

Writing this singular behavior in distributional form (see Refs. [21,32]), the boundary condition in (20) becomes

$$\partial_x S_1 = \frac{4\beta}{R} \sum_{n=1}^N \frac{b_n \delta(\theta_0 - \theta_n)}{\sin(\theta_n)} \delta(\varphi_0 - \varphi_n), \quad x = R. \qquad (24)$$

B. Effective trapping rate κ

To derive a one-dimensional approximation to $S(x, \theta, \varphi, t)$, we average over the orientations (θ, φ),

$$\overline{S}(x, t) := \frac{1}{(4\pi)^{N+1}} \int_{\Omega_0^{N+1}} S(x, \theta, \varphi, t) \, d\Sigma, \qquad (25)$$

where $d\Sigma := \prod_{n=0}^N \sin \theta_n \, d\theta_n \, d\varphi_n$. Note that $\overline{S}(x, t)$ is the survival probability conditioned that $X(0) = x$ and $(\Theta(0), \Phi(0))$ is uniformly distributed on Ω_0^{N+1}. It follows directly from the boundary value problem satisfied by S in (11)–(15) that $\overline{S}$ must satisfy

$$\partial_t \overline{S} = D_{\text{tr}} \partial_{xx} \overline{S}, \quad x \in (R, L + R), \; t > 0,$$

with the initial condition $\overline{S} = 1$. Further, $\overline{S}$ satisfies either (13) or (14), depending on whether $L < \infty$ or $L = \infty$.

Next, we want to derive an effective Robin boundary condition that $\overline{S}$ satisfies at $x = R$. To find this condition, we first define $\kappa(t)$ to be the ratio

$$\kappa(t) := \frac{D_{\text{tr}} \partial_x \overline{S}(R, t)}{\overline{S}(R, t)} > 0, \qquad (26)$$

so that it is a tautology that $\overline{S}$ satisfies the Robin boundary condition at $x = R$,

$$D_{\text{tr}} \partial_x \overline{S} = \kappa(t) \overline{S}, \quad x = R.$$

We then use the definition of $\kappa(t)$ in (26) to derive an explicit, time-independent formula for $\kappa(t)$ as $\varepsilon \to 0$.

In particular, by (26) and the definition of $\overline{S}$ in (25), we have

$$\kappa(t) = \frac{D_{\text{tr}} \partial_x \int_{\Omega_0^{N+1}} S(R, \theta, \varphi, t) \, d\Sigma}{\int_{\Omega_0^{N+1}} S(R, \theta, \varphi, t) \, d\Sigma}. \tag{27}$$

Now (18) implies that the integral in the denominator in (27) converges to $(4\pi)^{N+1}$ as $\varepsilon \to 0$. Further, interchanging the derivative with the integral in the numerator in (27) and using the outer expansion in (19) yields

$$\kappa(t) \sim \frac{\varepsilon D_{\text{tr}} \int_{\Omega_0^{N+1}} \partial_x S_1(R, \theta, \varphi, t) \, d\Sigma}{(4\pi)^{N+1}}, \quad \text{as } \varepsilon \to 0. \tag{28}$$

Next, the boundary condition (24) simplifies (28) to

$$\kappa(t) \sim \frac{\varepsilon \beta D_{\text{tr}}}{\pi R} \sum_{n=1}^{N} b_n, \quad \text{as } \varepsilon \to 0.$$

Finally, if we define the average,

$$\overline{b} := \frac{1}{N} \sum_{n=1}^{N} b_n,$$

then on using the definition of β in (21), we find that the trapping rate is independent of time and is given by

$$\kappa(t) \sim \kappa := \frac{\varepsilon N \overline{b}}{\pi R} \sqrt{D_{\text{tr}}(R^2 D_{\text{rot}} + D_{\text{pat}})}, \quad \text{as } \varepsilon \to 0. \tag{29}$$

If the patches have a common radius $a = \varepsilon R$ (and thus $b_n = \overline{b} = 1$), then (29) reduces to (2).

IV. NUMERICAL SIMULATION

A. Stochastic simulation algorithm

In this section, we perform numerical simulations to investigate the accuracy of our trapping rate in (29). Before giving the results of these simulations in the subsections below, we first describe our stochastic simulation algorithm.

We simulate the $(2N + 3)$-dimensional stochastic process $(X(t), \Theta(t), \Phi(t))$ in (7). This entails simulating the three SDEs in (4) and the $2N$ SDEs in (6). Further, this includes simulating the reflection of $X(t)$ at $x = L + R$ (the right wall of the slab) and either the reflection or absorption of $X(t)$ at $x = R$ (the trapping surface), depending on the orientation of the $2(N + 1)$ angles $(\Theta(t), \Phi(t)) \in \Omega_0^{N+1}$ when $X(t)$ hits $x = R$.

We simulate these SDEs using the Euler-Maruyama method [33]. To increase computational efficiency, we use either a large time step (denoted Δt_{big}) or a small time step (denoted Δt_{small}), depending on the distance between $(X(t), \Theta_0(t), \Phi_0(t))$ and the nearest absorbing patch $(R, \Theta_n(t), \Phi_n(t))$. Unless otherwise noted, we take $\Delta t_{\text{big}} = 10^{-5}$ and $\Delta t_{\text{small}} = 10^{-8}$. Our numerical method is similar to the method used in Ref. [21].

In all simulations, we take $D_{\text{tr}} = R = 1$, $L = 4$, and $X(0) = 2$. We also take $b_n = 1$ for all $n \in \{1, \ldots, N\}$ so that all the patches have the same size. We take the initial particle orientation $(\Theta_0(0), \Phi_0(0))$ to be uniformly distributed. Further, we initially place the N patches, $\{(\Theta_n(0), \Phi_n(0))\}_{n=1}^{N}$, on the particle according to the Fibonacci lattice [13], which is merely a simple way to homogeneously distribute points on a sphere.

We use this numerical algorithm to generate many independent realizations of the binding time τ in (8). From this numerical data, we then compute an empirical survival probability $S_{\text{emp}}(t)$. Specifically, if

$$0 < \tau_1 \leqslant \tau_2 \leqslant \cdots \leqslant \tau_{M-1} \leqslant \tau_M < \infty$$

denote M independent realizations of the binding time generated from the numerical algorithm, then the empirical survival probability is defined by $S_{\text{emp}}(0) = 1$,

$$S_{\text{emp}}(\tau_m) = 1 - \frac{m}{M}, \quad m \in \{1, \ldots, M\},$$

and $S_{\text{emp}}(t) = 0$ for $t \geqslant \tau_m$, with linear interpolation at all other times. For a large number of realizations ($M \gg 1$) and small discrete time steps ($\Delta t_{\text{big}} \ll 1$ and $\Delta t_{\text{small}} \ll 1$), it follows that $S_{\text{emp}}(t)$ approximates the survival probability in (9) for the initial conditions $(X(0), \Theta(0), \Phi(0))$ described in the previous paragraph.

In the following subsections, we compare S_{emp} to the survival probability $\overline{S}$ obtained from the one-dimensional PDE [(16) and (17)] where κ is given by (29). This one-dimensional PDE can be solved either analytically in terms of an explicit infinite series or numerically with standard software. We solve it using a numerical PDE solver in Matlab called `pdepe` [34].

B. Match full distribution

In Fig. 3, we plot S_{emp} and $\overline{S}$ and find very close agreement. In this plot, we set $D_{\text{rot}} = 0$, vary D_{pat}, and take $N = 50$ patches of radius $\varepsilon = 10^{-2}$. To quantify the agreement
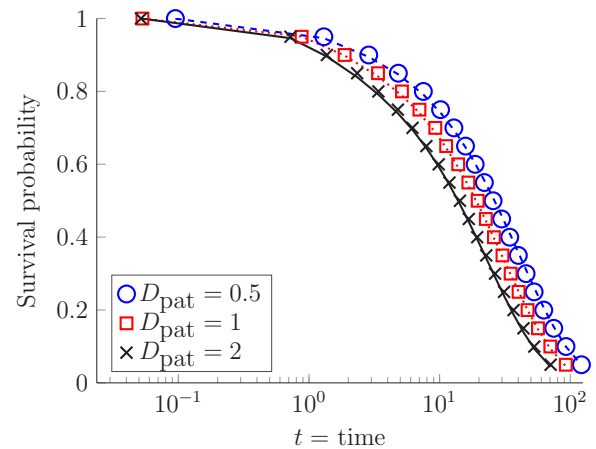
FIG. 3. Curves are the survival probability $\overline{S}$ using κ in (29), and the markers are the empirical survival probability S_{emp} computed from Monte Carlo simulations of the full stochastic process in (7). Here $\varepsilon = 10^{-2}$, $N = 50$, $D_{\text{rot}} = 0$, and $M = 4 \times 10^3$ trials for each value of $D_{\text{pat}} \in \{0.5, 1, 2\}$.
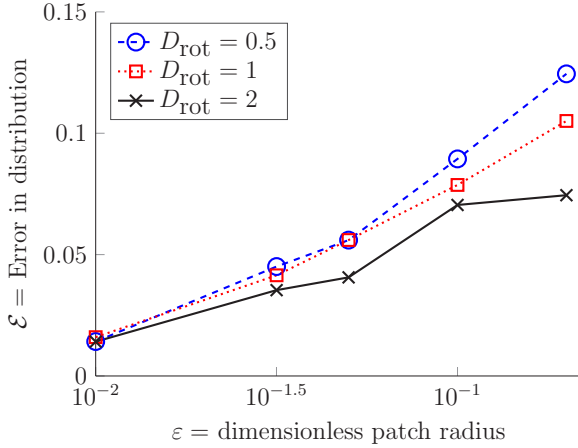
FIG. 4. The error in distribution $\mathcal{E}$ in (30) as a function of ε for different values of the rotational diffusivity D_{rot}. Here $N = 50$, $D_{\mathrm{pat}} = 0$, and $M = 10^4$ trials for each value of $\varepsilon \in \{10^{-2}, 10^{-1.5}, 0.5, 0.1, 0.2\}$ and $D_{\mathrm{rot}} \in \{0.5, 1, 2\}$.

between S_{emp} and $\overline{S}$, we define the error in distribution,

$$\mathcal{E} := \sup_{t \geqslant 0} |S_{\mathrm{emp}}(t) - \overline{S}(t)| \geqslant 0, \qquad (30)$$

which is the so-called Kolmogorov-Smirnov distance [35]. For the three sets of parameters in Fig. 3, the error is at most $\mathcal{E} = 0.015$.

In Fig. 4, we plot the error in distribution $\mathcal{E}$ in (30) as a function of the patch radius ε for different values of D_{rot}. From this plot, we see that $\mathcal{E}$ decreases from about $\mathcal{E} \approx 0.1$ when $\varepsilon = 0.2$ to about $\mathcal{E} \approx 0.015$ when $\varepsilon = 10^{-2}$.

These results confirm the analysis of Sec. III that using the effective trapping rate κ in (29) in the homogenized one-dimensional PDE [(16) and (17)] closely approximates the $(2N + 3)$-dimensional, anisotropic PDE in (11)–(15). In particular, the effective trapping rate κ allows us to capture the full probability distribution of the binding time τ in (8) (rather than just the mean of τ, for example). Hence, we emphasize that the trapping rate κ can be used in both steady-state and time-dependent problems (like the one above).

C. Optimal trapping rate

In the subsection above, we computed the error in distribution $\mathcal{E}$ in (30) between the empirical survival probability S_{emp} and the survival probability $\overline{S}$ obtained from solving the homogenized one-dimensional PDE [(16) and (17)] with trapping rate κ in (29). We now determine how our theoretical trapping rate κ in (29) compares to a numerically computed optimal trapping rate κ_{opt}.

That is, for a given empirical survival probability S_{emp} calculated from many Monte Carlo trials, we first compute the error in distribution $\mathcal{E}$ between S_{emp} and $\overline{S}$ for a broad range of trapping rates κ. We then define κ_{opt} to be the trapping rate that minimizes the error $\mathcal{E}$.

To illustrate, the black curve in Fig. 5(a) gives the error $\mathcal{E}$ between S_{emp} and $\overline{S}$ for trapping rate κ ranging from 0.05 to 0.3. We emphasize that this curve is generated merely by plugging in a range of numerical values for κ into the
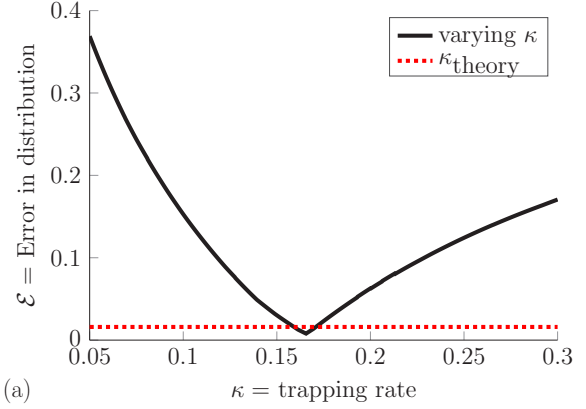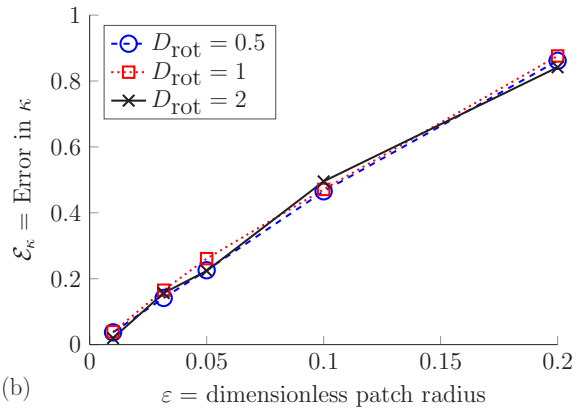
FIG. 5. Comparing the theoretical trapping rate in (29) and a numerically computed optimal trapping rate. (a) The black curve gives the error $\mathcal{E}$ in (30) between S_{emp} and $\overline{S}$ for trapping rates κ ranging from 0.05 to 0.3. The dashed red curve is the error $\mathcal{E}$ when the theoretical trapping rate in (29) is used. We take $\varepsilon = 10^{-2}$, $N = 50$, $D_{\mathrm{rot}} = 1$, $D_{\mathrm{pat}} = 0$, and $M = 10^4$ trials. (b) The error in κ in (31) as a function of ε for different values of D_{rot}. The parameters are as in Fig. 4.

one-dimensional PDE [(16) and (17)] and calculating the error $\mathcal{E}$. This curve has a sharp minimum at $\kappa_{\mathrm{opt}} \approx 0.17$. For the parameter values in this plot (see the figure caption), our theoretical trapping rate in (29) is $\kappa \approx 0.16$. We thus define the "error in κ" to be

$$\mathcal{E}_{\kappa} := \frac{|\kappa_{\mathrm{opt}} - \kappa|}{\kappa_{\mathrm{opt}}}, \qquad (31)$$

which in the case of Fig. 5(a) is about $\mathcal{E}_{\kappa} \approx 0.039$.

In Fig. 5(b), we plot $\mathcal{E}_{\kappa}$ in (31) as a function of ε for different values of D_{rot}. Importantly, this figure shows a linear decay of $\mathcal{E}_{\kappa}$ which validates that our theoretical trapping rate in (29) does indeed capture the leading-order behavior of the optimal trapping rate as $\varepsilon \to 0$. Furthermore, the linear decay in Fig. 5(b) further suggests that the next order correction to the trapping rate is $\mathcal{O}(\varepsilon^2)$, which is consistent with some boundary homogenization results on other problems [8,9,12].

V. RANGE OF VALIDITY

In this section, we discuss the parameter regimes and geometries in which boundary homogenization with the trapping rate κ in (29) is valid.

A. Parameter regimes

Recall that we derived the trapping rate in (29) in the limit $\varepsilon = a/R \to 0$. That is, if we fix the values of the other parameters (N, D_{tr}, D_{rot}, D_{pat}, etc.), then the trapping rate is valid for sufficiently small ε. Of course, the value of ε that is "sufficiently small" depends on the values of the other parameters (as well as what error tolerance is acceptable in order for the homogenization to be considered valid).

To estimate how the accuracy depends on the various parameters, first note that the asymptotic argument in Sec. III requires the patches to be well separated. More precisely, if N patches are approximately evenly distributed on a sphere of radius R, and l_0 is half the average distance between the centers of nearest-neighbor patches, then we have for large N

$$N\pi l_0^2 \approx 4\pi R^2.$$

Hence, requiring the patches to be well separated means

$$a \ll l_0 \approx 2R/\sqrt{N}. \tag{32}$$

Note that squaring (32) implies that the fraction of the particle's surface covered by patches is small, $Na^2/(4R^2) \ll 1$, which is commonly assumed in asymptotic analysis of spheres covered by absorbing patches [12].

Furthermore, the analysis in Sec. III used the fact that the particle becomes perfectly reflecting in the limit $\varepsilon \to 0$. In terms of the homogenized boundary condition (17), the particle becomes perfectly reflecting when the following dimensionless trapping rate is small,

$$\overline{\kappa} := \frac{\kappa R}{D_{\text{tr}}} = \frac{\varepsilon \beta N}{\pi} \ll 1. \tag{33}$$

Hence, putting (32) and (33) together yields the following sufficient condition to ensure high accuracy of homogenization with κ in (29):

$$\varepsilon \ll \min\left\{\frac{\pi}{\beta N}, \frac{2}{\sqrt{N}}\right\}. \tag{34}$$

Of course, for any fixed patch size $\varepsilon > 0$, the condition in (34) can be violated by taking $N \to \infty$ and/or $\beta \to \infty$. Hence, the asymptotic argument that yielded the trapping rate κ in (29) fails in either one of these limits. However, it turns out that homogenization with the trapping rate κ in (29) is valid in these limits.

To see this, first note that the particle becomes perfectly absorbing as $N \to \infty$, since the particle is completely covered in patches in this limit. Since the trapping rate in (29) is linear in N, it produces this desired large N behavior. Similarly, the particle becomes perfectly absorbing as $\beta \to \infty$, since the patches exhaustively explore their orientations before the particle diffuses away from the wall. This is because $R^2 D_{\text{rot}} + D_{\text{pat}}$ controls the patch orientation dynamics, and D_{tr} controls the translation of the particle (see Ref. [21] for more on this phenomenon). Since the trapping rate in (29) is linear in β, it produces this desired large β behavior.

Summarizing, we expect that homogenization with κ in (29) is most accurate if either (i) the condition in (34) holds (and thus $\overline{\kappa} \ll 1$) or (ii) $\overline{\kappa} \gg 1$. We illustrate this in Fig. 6, where we plot the error in distribution $\mathcal{E}$ in (30) as a function of κ for different values of ε. In this plot, we vary κ by varying
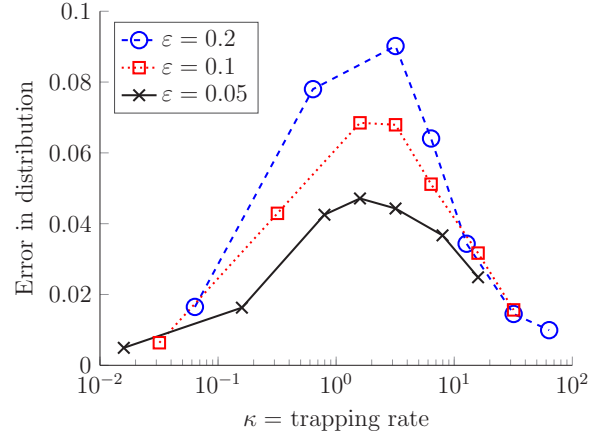
FIG. 6. Error in distribution $\mathcal{E}$ in (30) as a function of κ in (29) for different values of ε. Here $D_{\text{rot}} = 1$, $D_{\text{pat}} = 0$, $\Delta t_{\text{big}} = 10^{-3}$, $\Delta t_{\text{small}} = 10^{-6}$, and $M = 10^5$ trials for each value of $\varepsilon \in \{0.05, 0.1, 0.2\}$ and $N \in \{1, 10, 50, 100, 200, 500, 1000\}$.

N, and $\kappa = \overline{\kappa}$ since we take $R = D_{\text{tr}} = 1$. This plot illustrates the expected behavior, in that the error is a nonmonotonic function of κ, peaking at $\kappa \approx 1$ and decaying for both $\kappa \ll 1$ and $\kappa \gg 1$. Further, the peaks of the curves decay as ε decreases.

The patchy particle in our analysis could model a protein with small binding sites [15], a patchy colloid or nanoparticle with small reactive patches [16,17], or a cell with small surface receptors [1]. By assuming the patches are small compared to the particle ($\varepsilon \ll 1$), our analysis follows previous work. For example, Refs. [36–38] model protein interactions and consider ε between approximately 0.02 and 0.1, set N to be either 1 or 4 and take $\beta = \sqrt{3/4}$ by Stokes-Einstein [see (39) below], which puts the system in (or at least close to) the parameter regime in (34). For patchy nanoparticles, Ref. [16] takes $\varepsilon \approx 0.01$, sets N to be 1 or 2, and varies β between $\sqrt{3} \times 10^{-1}$ and $\sqrt{3} \times 10^{1}$, which again puts the system in (or at least close to) the parameter regime in (34).

B. The case $D_{\text{rot}} = D_{\text{pat}} = 0$

Our results assume that $D_{\text{rot}} + D_{\text{pat}} > 0$ to ensure that the particle "forgets" its initial patch orientation. Indeed, in the trivial case that $D_{\text{rot}} = D_{\text{pat}} = 0$, the behavior of the particle depends critically on the initial patch orientation. Specifically, if a patch is initially aligned with the absorbing wall, then the wall immediately absorbs the particle on contact. Otherwise, the particle will never be absorbed.

The analogous situation occurs in homogenization of patchy surfaces [Fig. 1(a)]. Indeed, the assumption that $D_{\text{rot}} + D_{\text{pat}} > 0$ is analogous to the standard assumption in previous works on homogenization of a patchy surface that there is nonzero diffusion in the directions parallel to the surface. To see this, consider the problem of a homogeneous particle and a patchy surface depicted in Fig. 1(a). Let $D_x > 0$ denote the particle diffusivity in the direction perpendicular to the surface, and let D_y and D_z denote the diffusivities in the directions parallel to the surface. Previous works assume $D_y > 0$, $D_z > 0$, which ensures that the particle "forgets" its initial

position in the plane parallel to the patchy surface (in fact, isotropic diffusion is typically assumed, $D_x = D_y = D_z > 0$). Analogously to the paragraph above, in the trivial case $D_y = D_z = 0$, the surface immediately absorbs the particle on contact if the particle is initially aligned to a patch in the plane parallel to the surface. Otherwise, the particle will never be absorbed.

C. Curved absorbing wall

Recall that we derived our results assuming the absorbing left wall is flat [see Fig. 1(b)]. It is natural to ask whether our results remain valid if the wall has some curvature. A smoothly varying wall introduces a new length scale to the problem, $R_c > 0$, which is the wall's characteristic radius of curvature. Naturally, this radius of curvature must be much greater than the radius of the particle, $R_c \gg R$, so that the wall is locally flat at the length scale of the particle.

In addition, the particle must forget its patch orientation over timescales in which the wall curvature affects the particle. Otherwise, the wall curvature would affect the patch orientation relative to the wall. To illustrate, Fig. 7 depicts a particle whose patch is initially not aligned with the wall but becomes aligned after particle translation, due to the wall curvature.

To prevent the situation in Fig. 7, first notice that the wall is effectively flat over timescales much less than $t_c := R_c^2 / D_{\text{tr}}$. That is, over a timescale much less than t_c, the particle moves a length scale over which the wall is effectively flat. Since the patches become completely reoriented over the timescale

$$t_r = \frac{R^2}{R^2 D_{\text{rot}} + D_{\text{pat}}},$$

requiring that $t_r \ll t_c$ ensures that the particle forgets its patch orientation before it is affected by the wall curvature. Therefore, our results remain valid in the case of a smoothly varying wall, as long as $R_c \gg R$ and

$$\frac{t_c}{t_r} = \frac{R^2 D_{\text{rot}} + D_{\text{pat}}}{D_{\text{tr}}} \frac{R_c^2}{R^2} = \beta^2 \frac{R_c^2}{R^2} \gg 1. \tag{35}$$

FIG. 7. The thick black curve depicts a curved absorbing left wall. Here (35) is not satisfied, and the wall curvature affects the patch orientation relative to the wall.

VI. DISCUSSION

We have found an explicit formula describing the rate that a diffusing patchy particle binds to a surface. This formula reveals how the binding rate depends on the translational and rotational diffusivities of the particle and the diffusivity of the patches. Mathematically, we formulated the problem in terms of a high-dimensional, time-dependent, anisotropic diffusion equation and analyzed this system using matched asymptotic analysis [12,21]. This analysis yielded the effective trapping rate in (2). We used numerical simulations to validate this formula across a range of parameter values.

Importantly, the trapping rate in (2) can be used for modeling either a single particle or a concentration of noninteracting particles and can be applied in both steady-state and time-dependent problems. Indeed, we found that using the trapping rate in (2) in a one-dimensional diffusion equation can capture the full probability distribution of the binding time of a single particle. For some recent works emphasizing the importance of the full distribution of binding times in the context of biochemistry, see Refs. [39–43].

To compare our effective trapping rate to previous work, let

$$\sigma := \frac{N a^2}{4 R^2}$$

denote the fraction of the particle surface covered by patches. Previous works [7] have written the effective trapping rate in the form

$$\kappa = \frac{4 D_{\text{tr}}}{\pi a} F(\sigma), \tag{36}$$

where $F(\sigma)$ is some dimensionless function of σ.

For the case of a homogeneous particle binding to a patchy surface [see Fig. 1(a)], the effective trapping rate can be written in the form (36) if

$$F_{\text{bp}}(\sigma) = \sigma. \tag{37}$$

Equation (37) is the leading-order behavior for $\sigma \ll 1$ [1]; for higher-order corrections see Refs. [6,7,12]. For a patchy particle binding to a homogeneous surface [see Fig. 1(b)], we found that the trapping rate (2) has the form (36) with

$$F(\sigma) = \beta \sigma, \quad \text{where } \beta := \sqrt{\frac{R^2 D_{\text{rot}} + D_{\text{pat}}}{D_{\text{tr}}}}. \tag{38}$$

Comparing (37) and (38), we see that the leading-order behavior of the trapping rate for (a) a homogeneous particle binding to a patchy surface or (b) a patchy particle binding to a homogeneous surface differs by the factor $\beta \in (0, \infty)$. Notice that β is a dimensionless factor comparing the translational diffusivity, D_{tr}, to the effective diffusivity governing the orientation of the patches, $R^2 D_{\text{rot}} + D_{\text{pat}}$.

If we take $D_{\text{pat}} = 0$ and assume the Stokes-Einstein relation for the particle's translational diffusivity D_{tr} and rotational diffusivity D_{rot}, then it follows that

$$\beta = \sqrt{3/4} \approx 0.87, \tag{39}$$

meaning that (38) corresponds to a slightly slower trapping rate than (37). However, if the Stokes-Einstein relation coupling D_{tr} and D_{rot} breaks down (or $D_{\text{pat}} > 0$), then β can

differ markedly from $\sqrt{3/4}$. Indeed, there are many situations in which the Stokes-Einstein relation breaks down, as D_{tr} and D_{rot} can be independently altered by molecular crowding agents or via external fields [16,44–46].

Hence (38) highlights the importance of relative translational and rotational diffusivities in the binding of a patchy particle. Determining the contribution of rotational diffusion to association rates has a long history [44,47], dating back at least to Ref. [48]. In contrast to the present work, prior works have focused on the binding of a pair of particles and have tended to either (i) rely on computer simulations [16,36,49,50] or (ii) consider a single patch and use heuristic approximations to make the problem amenable to standard methods [37,38,51]. The analytical methods we employed are similar to Refs. [12,21], in which the authors studied the rate that particles diffusing exterior to a sphere reach small targets on the sphere's surface. In the present work, our analysis required modifying these methods to account for the particular anisotropic diffusion introduced by the geometry of our problem, see Fig. 2.

In closing, this work introduces a conceptually new, first-principles derivation of the so-called partially absorbing boundary condition (also known as a partially reactive, Robin, third type, impedance, radiation, or convective condition [52–55]). In contrast to previous derivations where the boundary condition arises from properties of the boundary [56–60], the boundary condition in the present work arises from a property of the particle.

ACKNOWLEDGMENTS

[1] H. C. Berg and E. M. Purcell, Biophys. J. **20**, 193 (1977).

[2] F. J. Keil, Catal. Today **53**, 245 (1999).

[3] B. R. Scharifker, J. Electroanal. Chem. Interfacial Electrochem. **240**, 61 (1988).

[4] H. T. Brown and F. Escombe, Philos. Trans. Roy. Soc. Lond. B **193**, 223 (1900).

[5] A. Wolf, W. R. L. Anderegg, and S. W. Pacala, Proc. Natl. Acad. Sci. USA **113**, E7222 (2016).

[6] R. Zwanzig, Proc. Natl. Acad. Sci. USA **87**, 5856 (1990).

[7] A. Berezhkovskii, Y. Makhnovskii, M. Monine, V. Zitserman, and S. Shvartsman, J. Chem. Phys. **121**, 11390 (2004).

[8] A. M. Berezhkovskii, M. I. Monine, C. B. Muratov, and S. Y. Shvartsman, J. Chem. Phys **124**, 036103 (2006).

[9] C. Muratov and S. Shvartsman, Multiscale Model Simul. **7**, 44 (2008).

[10] A. F. Cheviakov, A. S. Reimer, and M. J. Ward, Phys. Rev. E **85**, 021131 (2012).

[11] L. Dagdug, M. Vázquez, A. Berezhkovskii, and V. Zitserman, J. Chem. Phys. **145**, 214101 (2016).

[12] A. E. Lindsay, A. J. Bernoff, and M. J. Ward, Multiscale Model Simul. **15**, 74 (2017).

[13] A. J. Bernoff and A. E. Lindsay, SIAM J. Appl. Math. **78**, 266 (2018).

[14] A. Bernoff, A. Lindsay, and D. Schmidt, Multiscale Model. Simul. **16**, 1411 (2018).

[15] H. C. R. Klein and U. S. Schwarz, J. Chem. Phys. **140**, 184112 (2014).

[16] A. C. Newton, J. Groenewold, W. K. Kegel, and P. G. Bolhuis, Proc. Natl. Acad. Sci. USA **112**, 15308 (2014).

[17] C. J. Roberts and M. A. Blanco, J. Phys. Chem. B **118**, 12599 (2014).

[18] D. A. Lauffenburger and J. Linderman, *Receptors: Models for Binding, Trafficking, and Signaling* (Oxford University Press, Oxford, 1993).

[19] G. A. Pavliotis, *Stochastic Processes and Applications* (Springer, Berlin, 2016).

[20] C. Gardiner, *Stochastic Methods: A Handbook for the Natural and Social Sciences*, 4th ed., Springer Series in Synergetics, Vol. 13 (Springer, Berlin, 2009).

[21] S. D. Lawley and C. E. Miles, SIAM J. Appl. Math. **79**, 1124 (2019).

[22] A. F. Cheviakov and M. J. Ward, Math. Comput. Model **53**, 1394 (2011).

[23] A. F. Cheviakov, M. J. Ward, and R. Straube, Multiscale Model Simul. **8**, 836 (2010).

[24] D. Coombs, R. Straube, and M. Ward, SIAM J. Appl. Math. **70**, 302 (2009).

[25] M. J. Ward, W. D. Henshaw, and J. B. Keller, SIAM J. Appl. Math **53**, 799 (1993).

[26] M. J. Ward and J. B. Keller, SIAM J. Appl. Math **53**, 770 (1993).

[27] A. Amitai, I. Kupka, and D. Holcman, Phys. Rev. Lett. **109**, 108302 (2012).

[28] P. C. Bressloff and S. D. Lawley, Multiscale Model Sim. **13**, 1420 (2015).

[29] P. C. Bressloff and S. D. Lawley, Phys. Rev. E **92**, 062117 (2015).

[30] V. Fabrikant, *Applications of Potential Theory in Mechanics: A Selection of New Results*, Vol. 51 (Kluwer Academic Publishers, Dordrecht, 1989).

[31] H. Weber, J. reine angew. Math. **75**, 75 (1873).

[32] S. D. Lawley and C. E. Miles, J. Nonlin. Sci., 1 (2019).

[33] P. E. Kloeden and E. Platen, *Numerical Solution of Stochastic Differential Equations*, corrected edition (Springer, Berlin, 1992).

[34] MATLAB, version 9.3 (R2017b) (The MathWorks Inc., Natick, MA, 2017).

[35] Y. Dodge, *The Concise Encyclopedia of Statistics* (Springer Science & Business Media, New York, 2008).

[36] S. H. Northrup and H. P. Erickson, Proc. Natl. Acad. Sci. USA **89**, 3338 (1992).

[37] D. Shoup, G. Lipari, and A. Szabo, Biophys. J. **36**, 697 (1981).

[38] O. Berg, Biophys. J. **47**, 1 (1985).

[39] O. Bénichou, C. Chevalier, J. Klafter, B. Meyer, and R. Voituriez, Nat. Chem. **2**, 472 (2010).

[40] B. Meyer, C. Chevalier, R. Voituriez, and O. Bénichou, Phys. Rev. E **83**, 051116 (2011).

[41] D. S. Grebenkov, R. Metzler, and G. Oshanin, Phys. Chem. Chem. Phys. **20**, 16393 (2018).

[42] D. S. Grebenkov, R. Metzler, and G. Oshanin, Commun. Chem. **1**, 96 (2018).

[43] S. D. Lawley and J. B. Madrid, J. Chem. Phys. **150**, 214113 (2019).

[44] Y. Y. Kuttner, N. Kozer, E. Segal, G. Schreiber, and G. Haran, J. Am. Chem. Soc. **127**, 15138 (2005).

[45] C. Li, Y. Wang, and G. J. Pielak, J. Phys. Chem. B **113**, 13390 (2009).

[46] Y. Wang, C. Li, and G. J. Pielak, J. Am. Chem. Soc. **132**, 9392 (2010).

[47] O. G. Berg and P. H. von Hippel, Annu. Rev. Biophys. **14**, 131 (1985).

[48] K. Solc and W. Stockmayer, J. Chem. Phys. **54**, 2981 (1971).

[49] H.-X. Zhou, Biophys. J. **64**, 1711 (1993).

[50] A. H. Elcock, D. Sept, and J. A. McCammon, J. Phys. Chem. B **105**, 1504 (2001).

[51] K. Šolc and W. Stockmayer, Int. J. Chem. Kinet. **5**, 733 (1973).

[52] S. D. Lawley and J. P. Keener, SIAM J. Appl. Dyn. Syst. **14**, 1845 (2015).

[53] S. J. Chapman, R. Erban, and S. A. Isaacson, SIAM J. Appl. Math. **76**, 368 (2016).

[54] R. Erban and S. J. Chapman, Phys. Biol. **4**, 16 (2007).

[55] A. Singer, Z. Schuss, A. Osipov, and D. Holcman, SIAM J. Appl. Math **68**, 844 (2008).

[56] J. Filo, Arch. Math. **34**, 83 (1998).

[57] J. Filo and S. Luckhaus, J. Differ. Eq. **120**, 133 (1995).

[58] J. Filo and S. Luckhaus, J. Eur. Math. Soc. **2**, 217 (2000).

[59] A. Friedman, C. Huang, and J. Yong, Commun. Part. Differ. Eq. **20**, 59 (1995).

[60] O. Oleinik and T. Shaposhnikova, J. Math. Sci. **97**, 4014 (1999).